Published in final edited form as:
Neuroimage. 2014 December ; 103: 10–19. doi:10.1016/j.neuroimage.2014.09.006.

Mapping mean axon diameter and axonal volume fraction by MRI using temporal diffusion spectroscopy

Junzhong Xu[1,2,3,*], **Hua Li**[1,3], **Kevin D. Harkins**[1,2], **Xiaoyu Jiang**[1,2], **Jingping Xie**[1,2], **Hakmook Kang**[4], **Mark D. Does**[1,2,5], and **John C. Gore**[1,3,5,6]

[1]Institute of Imaging Science, Vanderbilt University, Nashville, TN 37232, USA

[2]Department of Radiology and Radiological Sciences, Vanderbilt University, Nashville, TN 37232, USA

[3]Department of Physics and Astronomy, Vanderbilt University, Nashville, TN 37232, USA

[4]Department of Biostatistics, Vanderbilt University, Nashville, TN 37203, USA

[5]Department of Biomedical Engineering, Vanderbilt University, Nashville, TN 37232, USA

[6]Department of Molecular Physiology and Biophysics, Vanderbilt University, Nashville, TN 37232, USA

Abstract

Mapping mean axon diameter and intra-axonal volume fraction may have significant clinical potential because nerve conduction velocity is directly dependent on axon diameter, and several neurodegenerative diseases affect axons of specific sizes and alter axon counts. Diffusion-weighted MRI methods based on the pulsed gradient spin echo (PGSE) sequence have been reported to be able to assess axon diameter and volume fraction non-invasively. However, due to the relatively long diffusion times used, e.g. > 20 ms, the sensitivity to small axons (diameter < 2 μm) is low, and the derived mean axon diameter has been reported to be overestimated. In the current study, oscillating gradient spin echo (OGSE) diffusion sequences with variable frequency gradients were used to assess rat spinal white matter tracts with relatively short effective diffusion times (1 – 5 ms). In contrast to previous PGSE-based methods, the extra-axonal diffusion cannot be modeled as hindered (Gaussian) diffusion when short diffusion times are used. Appropriate frequency-dependent rates are therefore incorporated into our analysis and validated by histology-based computer simulation of water diffusion. OGSE data were analyzed to derive mean axon diameters and intra-axonal volume fractions of rat spinal white matter tracts (mean axon diameter ~ 1.27 – 5.54 μm). The estimated values were in good agreement with histology, including the small axon diameters (< 2.5 μm). This study establishes a framework for quantification of nerve morphology using the OGSE method with high sensitivity to small axons.

[*]**Corresponding author**: Vanderbilt University Institute of Imaging Science, 1161 21st Avenue South, AA 1105 MCN, Nashville, TN 37232-2310, United States. Fax: + 1 615 322 0734., junzhong.xu@vanderbilt.edu (Junzhong Xu).

Keywords

diffusion; oscillating gradient; axon diameter; volume fraction; diffusion time; MRI

INTRODUCTION

Measurements of axon diameters in white matter are of considerable interest for studies of neural function in both research and clinical applications. For healthy myelinated nerves, it is well known that conduction velocity is directly proportional to axon diameter (Ritchie, 1982). In many inherited and acquired neurological disorders, axon damage has been reported to be size-dependent (Brun and Englund, 1986) . For example, small axons under ~3.3 μm diameter seem to be relatively more affected in multiple sclerosis than larger axons (Lovas et al., 2000). Glaucoma involves a primary injury in which large retinal ganglion cells are more vulnerable (Glovinsky et al., 1991), while the secondary degeneration of neural tissue with gradual loss of vision accompanies significant axon swelling (Payne et al., 2012). In addition, the extent of axonal swelling has been reported to be correlated with survival time after diffuse axonal injury, and the mean diameter of damaged axons depends on the severity and mode of the diffuse axonal injury (Wilkinson et al., 1999). Therefore, mapping axon diameter (AxD) may not only provide important insights into the pathophysiology of neural tissues, but also facilitate the diagnosis, evaluation or prediction of progression of some neural degenerative diseases at early stages. However, such histological information can currently be obtained only via invasive tissue biopsies, so it would be valuable to develop a non-invasive imaging technique to map AxD non-invasively.

Diffusion-weighted MRI (DWI) has been shown repeatedly to be able to probe biological tissue microstructure non-invasively, and hence may provide a means to measure quantitative microstructural information such as mean AxD *in vivo*. However, previous attempts, using conventional approaches, to correlate the transverse apparent diffusion coefficient (ADC) with mean AxD were not successful (Gullapalli et al., 2006; Schwartz et al., 2005a, 2005b). Simple conventional DWI metrics, such as ADC or fractional anisotropy (FA), do not provide specific information about AxD or intra-axonal volume fraction. More complex approaches such as **q**-space imaging, as proposed by Callaghan (Callaghan et al., 1991) and by Cory and Garroway (Cory and Garroway, 1990), involves Fourier transformation of the signal decay with respective to q (= $\gamma G\delta$, γ= gyromagnetic ratio of protons, G = gradient amplitude, and δ = duration of diffusion gradient) from which the displacement probability profile of water molecules can be obtained. This provides quantitative microstructural information (e.g. the mean pore size of porous media), and has also been successfully implemented for imaging nerve and white matter tracts, including bovine optic nerve (Assaf and Cohen, 2000), rat spinal cord (Anaby et al., 2013; Assaf et al., 2000) and mouse spinal cord (Ong and Wehrli, 2010; Ong et al., 2008). However, **q**-space imaging suffers one major drawback that, in order to accurately measure the size of small axons (e.g. diameter of 1 – 2 μm), very high q values and short gradient pulses must be used (Lätt et al., 2007), which requires extremely strong diffusion gradient strengths and high slew rates — e.g. 4800 G/cm gradient strength to reach $q_{max} = 0.82$ μm^{-1} (Ong et al., 2008). In practice, neural tissues, especially in the central nervous system, usually contain a large

fraction of small axons, so this in turn significantly limits the ability of **q**-space imaging to accurately quantify small axons *in vivo*. Another approach, the AxCaliber method, is based on the CHARMED model that assumes restricted diffusion in the intra-axonal space, hindered diffusion in the extra-axonal space, and no water exchange between these two compartments (Assaf et al., 2004). This method probes biological tissues with multiple diffusion times and *q*-values, and the AxD distribution can be obtained *in vitro* (Assaf et al., 2008) and *in vivo* (Barazany et al., 2009) based on *a priori* mathematical models. The ActiveAx method was developed to measure the indices of mean AxD instead of the AxD distribution so that the method is more clinically feasible due to reduced scanning time, although the mean AxD is significantly overestimated (Alexander et al., 2010). All the approaches above use conventional pulsed gradient spin echo (PGSE) pulse sequences which usually employ relatively long diffusion times *in vivo*, e.g. > 20 ms. The root mean square displacement of water molecules during such intervals is usually much larger than typical AxD's (1 – 5 μm) and so the sensitivity to small axons is low. For example, it has been reported that the ActiveAx method cannot identify axons with diameters smaller than 2.5 μm with a maximum gradient strength 30 G/cm (Dyrby et al., 2013). To compensate, PGSE-based methods usually need to use very large *q* or b values, but these are limited by practical scanning times, SNR and hardware performance (Ong et al., 2008).

Conceptually, the sensitivity to small axons may be enhanced by reducing the diffusion time. Oscillating gradient spin echo (OGSE) pulse sequences have been proposed to achieve significantly shorter diffusion times, e.g. 1 – 2 ms *in vivo*, with alleviated requirements for hardware performance (Gross and Kosfeld, 1969). This method typically replaces bipolar diffusion gradients with oscillating diffusion-sensitizing gradients, and by varying the oscillation frequency, a temporal diffusion spectrum (Parsons Jr. et al., 2006) can be obtained to provide more comprehensive information of biological tissues (Gore et al., 2010; Xu et al., 2012b). The OGSE method has been successfully implemented to measure the surface-to-volume ratio of porous media (Parsons Jr. et al., 2006), and to characterize cerebral ischemia (Does et al., 2003), intra-cellular microstructural variations (Colvin et al., 2011a; Xu et al., 2011b, 2009a) and tumor response to treatment (Colvin et al., 2011b; Xu et al., 2012b). Recently, there has been an increasing interest in applying OGSE methods in neuroimaging. For example, the fractional anisotropy (FA) obtained using OGSE sequences was found to be dependent on the gradient frequency (diffusion time) in fixed monkey brain (Xu et al., 2010), which was later confirmed in a series of studies in fixed mouse brain (Aggarwal et al., 2012), live rat brain (Kershaw et al., 2013), and human brain (Baron and Beaulieu, 2014; Van et al., 2014). Quantitative characterization of mean axon size using the OGSE method has been proposed and validated with computer simulations (Xu et al., 2009b). Two attempts have been reported to map axon size of fixed tissues using OGSE-like diffusion sequences (Shemesh et al., 2013; Siow et al., 2013). However, the results of these two studies were not validated with histology; and more importantly, the intra-axonal volume fraction, one of the important indicators of white matter morphology, was not obtained. In the current study, we report a more comprehensive study using the OGSE method to obtain histology-validated quantitative microstructural information on nerves, including both mean axon size and axonal space volume fraction. We emphasize that, due to the short diffusion times achievable with the OGSE method, the detection sensitivity to

small axons is expected to increase significantly. This suggests that the OGSE method may be a preferred approach to measure AxD, especially when relatively small axons make up a large fraction of tracts in the nervous system.

Fixed rodent spinal cord has been extensively used as a model system to test the accuracy of quantitative diffusion MRI methods due to its simple geometric organization and the varying mean AxD's across different white matter tracts (Assaf et al., 2000; Chin et al., 2004; Komlosh et al., 2013; Ong and Wehrli, 2010; Ong et al., 2008; Schwartz et al., 2005a, 2005b). In the current study, OGSE pulse sequences were implemented to measure the mean AxD of fixed rodent spinal cord white matter tracts. Histological-image-based computer simulations were performed to investigate intra- and extra-axonal diffusion individually based on realistic white matter morphology. Combined with previously developed analytical signal models for restricted structures (Xu et al., 2009b) and a time-dependent diffusion model for random packing (Novikov et al., 2012, 2011), the appropriate analyses for intra- and extra-axonal diffusion were derived for practical measurements. These analyses were then used to fit OGSE diffusion data to estimate the mean AxD of fixed rat spinal cords *ex vivo*, and then compared with histological measurements. The results show that the OGSE method provides an accurate measurement of mean axon diameter, including small axons (~ < 2.5 μm). The current OGSE results and previously published **q**-space and AxtiveAx results are also compared briefly.

MATERIALS AND METHODS

Theory

In contrast to conventional PGSE methods, OGSE sequences employ oscillating diffusion-sensitizing gradients with variable frequencies to measure a temporal diffusion spectrum, i.e. ADC(*f*), with respective to the oscillating gradient frequency *f*. Note that the effective diffusion time of each OGSE measurement is 1/(4*f*) for a cosine-modulated gradient waveform, which has been validated in neural tissues when only low b values were used (Portnoy et al., 2012). Therefore, higher frequencies result in shorter diffusion times during which water molecules encounter fewer restriction boundaries. The detailed theory of the OGSE method has been thoroughly reviewed previously (Gore et al., 2010).

We assume that the OGSE signals of white matter can be expressed as the sum of signals arising from intra- and extra-axonal spaces, namely,

$$S = f_{in} \cdot S_{in} + (1 - f_{in}) \cdot S_{ex}, \quad (1)$$

where f_{in} is the water volume fraction of intra-axonal space over the sum of intra- and extra-axonal spaces, and S_{in} and S_{ex} are the signal magnitudes per volume from the intra- and extra-axonal spaces, respectively. Note that the signal contribution from myelin water is ignored due to low T_2, low water concentration, low perpendicular diffusivity (Andrews et al., 2006; Harkins et al., 2012) and the relatively long echo times in the OGSE measurements. Eq.(1) also assumes that there is no water exchange between intra- and extra-axonal spaces, as suggested in the CHARMED model (Assaf et al., 2004).

Intra-axonal diffusion

Axons are usually modeled as parallel cylinders despite the significant variations of axon shape in realistic tissues. The CHARMED model assumes the AxDs obey a Gamma distribution (Assaf et al., 2008), while other models assume that the intra-axonal diffusion can be modeled as water molecules restricted inside parallel impermeable cylinders with a unique mean AxD (Alexander et al., 2010; Ford and Hackney, 1997; Ong and Wehrli, 2010; Szafer et al., 1995). The latter approach simplifies the mathematical complexity but preserves the basic feature of axonal structures, and hence is preferable for the current study. The analytical expressions of OGSE signals in some typical geometrical structures, e.g. cylinders and spheres, have been derived previously (Xu et al., 2009b). For OGSE measurements with cosine-modulated gradient waveforms, the analytical signal attenuation can be expressed as

$$S_{in}(G)=\exp\left\{-2(\gamma g)^2\sum_n \frac{B_n\lambda_n^2 D_{in}^2}{\left[\lambda_n^2 D_{in}^2+(2\pi f)^2\right]^2}\left\{\frac{\left[\lambda_n^2 D_{in}^2+(2\pi f)^2\right]}{\lambda_n D_{in}}\left[\frac{\delta}{2}+\frac{\sin(4\pi f\delta)}{8\pi f}\right]-1\right.\right.$$
$$\left.\left.+\exp(-\lambda_n D_{in}\delta)+\exp(-\lambda_n D_{in}\Delta)\left[1-\cosh(\lambda_n D_{in}\delta)\right]\right\}\right\} \quad (2)$$

where D_{in} is the intra-cylinder diffusion coefficient, f is the oscillation frequency, δ is the gradient duration, Δ is the separation of two diffusion gradients, and λ_n and B_n are structure dependent parameters containing cylinder diameter (Xu et al., 2009b). The accuracy of Eq. (2) has been validated by computer simulations (Xu et al., 2009b) and later by NMR measurements using well-characterized phantoms consisting of hollow micro-capillaries (Li et al., 2014).

Extra-axonal diffusion

In previous PGSE-based diffusion studies, extra-axonal diffusion was usually considered as hindered (Gaussian) diffusion, and hence a constant diffusion coefficient D_{ex} can be assumed to be independent of diffusion time. Although the accuracy of such an assumption has been questioned (Novikov et al., 2012), it has been reported that reasonable results, e.g. mean axon size or axon size distribution, can be obtained based on this hindered diffusion approximation using PGSE-based methods (Assaf et al., 2008; Barazany et al., 2009; Ong and Wehrli, 2010). However, the extra-axonal diffusion cannot be simplified as a constant in OGSE measurements with short effective diffusion times. This is because the root mean square displacements associated with the short diffusion times are usually comparable to or even smaller than the mean restriction distance in the extra-axonal space, and hence the extra-axonal diffusion shows significant dependence on gradient frequencies (or diffusion times) (Novikov et al., 2012). Due to the geometrical complexity of the extra-axonal space, the accurate dependence of extra-axonal diffusion on frequency is not easy to obtain. Although attempts have been made to model extra-axonal diffusion with the OGSE method (Lam et al., 2014; Stepisnik et al., 2006), no previous OGSE studies have used a frequency-dependent extra-axonal diffusion model to analyze experimental data in order to accurately derive microstructural information on nerves from OGSE measurements.

It has been observed that, when a narrow range of relatively low frequencies is used, the ADC values obtained in OGSE measurements show a near linear dependence on the gradient frequency (Aggarwal et al., 2012; Xu et al., 2012a, 2012b). Novikov et al. provided

a theoretical explanation that the ADC of a completely randomly packed 2D system is linearly dependent on low frequencies (Novikov et al., 2012). Achievable frequencies in practical OGSE measurements are usually moderately low due to hardware limitations, so this theory may be valid for the extra-axonal space diffusion in OGSE measurements. In the current study, histology-based computer simulations were performed to validate whether the extra-axonal space diffusion coefficient $D_{ex}(f)$ can be modeled as a linear function of gradient frequency, namely,

$$S_{ex}=\exp\left[-b\cdot D_{ex}(f)\right]=\exp\left[-b\cdot(D_{ex0}+\beta_{ex}\cdot 2\pi f)\right], \quad (3)$$

where D_{ex0} is a constant and β_{ex} is the slope of $D_{ex}(f)$ with respective to frequency $2\pi f$, which contains microstructural size information but may not be simply related to any specific physical structure in the tissues (Novikov et al., 2014).

Tissue preparation

Six Sprague Dawley rats (275 – 350 g) were perfused, under deep anesthesia, through the left cardiac ventricle with phosphate buffer followed by 0.5% paraformaldehyde and 4% glutaraldehyde in phosphate buffer. Cervical spinal cord sections ≈ 1 cm in length were cut out and immediately placed in 0.5% paraformaldehyde and 4% glutaraldehyde in phosphate buffer for 48 hours. The samples were then washed in phosphate-buffered saline solution for at least 3 days prior to MRI study to wash out fixatives and restore T_2 (Shepherd et al., 2009). For each MRI scan, a sample was put inside a 5-mm NMR tube and immersed in fomblin to reduce susceptibility effects arising from air-tissue interfaces. Further details of the tissue preparation can be found in previous reports (Dula et al., 2010; Harkins et al., 2012).

Magnetic resonance imaging

All MRI experiments were performed on a 7T Varian DirectDrive horizontal imaging spectrometer (Santa Clara, CA) equipped with a 12-mm microgradient coil (Doty Scientific Inc., Columbia, SC). All images were acquired using a 4-shot echo-planar imaging sequence with a 1D navigator echo acquired before the data acquisition. The field-of-view = 5 × 5 mm. The matrix size = 64 × 64, and then zero-filled to 128 × 128, yielding an interpolated spatial resolution of 39.1 μm. TR = 4 sec, TE = 58 ms, and slice thickness = 2 mm. The diffusion gradients were apodized cosine waveforms with a duration of 20 ms and a separation of 24 ms. All diffusion gradients were applied perpendicular to the spinal cord tracts with five frequencies (50, 100, 150, 200, 250 Hz), each frequency employed five b values (0, 500, 1000, 1500, 2000 s/mm^2), and the maximum gradient strength used in the current study was 133 G/cm in x and y directions. The number of acquisitions averaged was chosen to be 80 to fulfill an overnight scan which took around 15 hours. The typical SNR of white matter tracts was around 200.

Histology

After MRI measurements, samples were dehydrated in graded ethanol and embedded in epoxy resin, and 1-μm-thick axial sections were cut at the middle of the spinal cord (where the MR image slice was acquired), and then stained with 1% Toluidine Blue solution.

Previous studies have observed a 10% decrease of cross-sectional area with the current tissue sample preparation protocol (Denef et al., 1979; Tang and Nyengaard, 1997), indicating the tissue shrinkage is not a significant factor in the current study. Digital images were acquired using oil immersion light microscopy (LM) at 75 nm × 75 nm resolution. However, note that the intrinsic optical resolution limit is actually ~200 nm using conventional lenses (van Putten et al., 2011). LM images were collected from six spinal white matter tracts of each fixed spinal cord, i.e. vestibulospinal tract (VST), fascisulus cuneatus (FC), rubrospinal tract (RST), reticulospinal tract (ReST), funiculus gracilis (FG), and dorsal corticospinal tract (dCST). Histological images were digitally smoothed with an edge-preserving anisotropic diffusion filter, enhanced with adaptive histogram equalization, and semi-automatically segmented using a region growing routine into regions of intra-, extra-axonal spaces, and myelin. Manual adjustments were performed to correct any misidentified regions and to add some thin paths that connect extra-axonal spaces. The histology section size was chosen to include ~200 or more axons in each histological section, i.e. 67.61×67.61 μm^2 for VST and FC, 45.11×45.11 μm^2 for RST and ReST, and 33.86×33.86 μm^2 for FG and dCST The area-weighted mean AxD (Alexander et al., 2010; Harkins et al., 2012) was obtained for each white matter tract, namely,

$$mean\ AxD = \frac{\sum_{n=1}^{N} d_n^3}{\sum_{n=1}^{N} d_n^2}, \quad (4)$$

where N is the total number of axons in each histological image, and d_n is the effective diameter of the nth axon. The volume fractions of intra-, extra-axonal spaces and myelin were also obtained from histology, and f_{in}, the volume fraction of intra-axonal space over the sum of intra- and extra-axonal spaces was calculated.

Histology-based computer simulations

The segmented histological images of all white mater tracts of all rat spinal cords were downsampled to a resolution of 0.1125×0.1125 μm, then used as input structures for computer simulations, similar to previous histology-based studies (Chin et al., 2002, 2004). The computer simulation used a Finite-Difference Time-Domain algorithm with a revised boundary condition and a parallel computing scheme for better accuracy and efficiency (Xu et al., 2007). The intrinsic diffusion coefficient of water molecules was assumed to be 1.0 μm^2/ms everywhere as suggested previously (Chin et al., 2002). Note that the sensitivity of diffusion experiments to the intracellular diffusion coefficient is actually low when the axon sizes are small as confirmed in previous microcapillary experiments (Li et al., 2014). The water exchange between different compartments was assumed to be negligible. Therefore, signals arising from intra- and extra-axonal spaces can be obtained separately from the simulations. All OGSE pulse sequence parameters were the same as in the measurements.

Two types of simulations were performed. The first type simulated the apparent diffusion spectra of intra- and extra-axonal spaces of six representative images, and then the spectra were fit to Eq.(2) and Eq.(3), respectively. By this means, the intra- and extra-axonal diffusion models proposed in the current study were validated. The second type simulated

the OGSE signals to mimic the OGSE measurements, and then fit the simulated signals to Eq.(1) to quantify mean AxD and f_{in}. It is valuable to investigate the detection resolution limit of the OGSE measurements, i.e. to assess over what mean AxD range the OGSE measurements can provide reliable fitting results. Usually, a broad range of mean AxD should be used, such as 0.5 – 10 μm used in previous studies (Dyrby et al., 2013). However, the histological mean AxD of all white matter tracts used in the current study ranged from 1.10 μm to 5.98 μm. In order to achieve a broader mean AxD range, each type of white matter tract (N=6) was randomly divided into three groups (two in each). One group kept the original spatial scale, while the other two either doubled or shrunk the original scale by half. By this means, we obtained input structures for computer simulation with realistic microstructural features (e.g. axon shape, volume fraction, packing density, etc.) but with a much broader mean AxD range (0.55 – 11.96 μm). This strategy is different from the previous method that used perfect cylinders and a fixed volume fraction (0.7) (Dyrby et al., 2013).

Data analysis

Regions of interest (ROI's) of gray matter and white matter were manually drawn on the T_2-weighted images of each spinal cord, and then OGSE signals with multiple b and frequency values were fit to Eq.(1) pixel-wise to obtain five parametric maps, i.e. AxD, f_{in}, D_{in}, D_{ex0}, and β_{ex}. In addition, ROI's of six different white matter tracts were manually drawn on fitted AxD maps from each spinal cord (yielding altogether 36 ROI's) for the ROI-based analysis and comparison with histology. Note that bilateral ROI's for e.g. VST and ReST were drawn and averaged to form one ROI for each tract. The constraints for fitting parameters were (parameter [lower bound, upper bound]): AxD [0.2, 10] μm, f_{in} [0, 1], D_{in} [0, 3] μm^2/ms, D_{ex0} [0, 3] μm^2/ms, and β_{ex} [0, 2] μm^2. Randomly-generated initial parameter values were used. To ensure the global minimum was reached, the fitting was repeated 50 times for each pixel and the analyses corresponding to the smallest fitting residuals were chosen as the final results. Bland-Altman plots were used to evaluate the differences in parameters of mean AxD and f_{in} fitted from OGSE measurements/simulations vs. those from histology. Because the six white matter tracts per animal are not independent of each other, linear mixed-effects models with compound symmetry structure of the correlation were employed to evaluate the relationship between histological mean AxD and all fitted parameters. By such means, the animal-specific dependence of each fitted parameter was taken into account. This analysis was performed with R statistical software version 3.0.2 (http://www.r-project.org/). For each model, histogram and scatter plot of residuals were visually inspected to assure the normality of each parameter and randomness of the error, respectively.

RESULTS

Histology

The mean axon diameters and intra-axonal volume fractions are shown in Table 1. The values and errors represent the mean and standard deviations across all six samples, respectively. The mean axon diameter decreases from 4.63 μm in VST to 1.39 μm in dCST, consistent with numerous previous publications (Harkins et al., 2012; Ong and Wehrli, 2010; Ong et al., 2008). Repeated measures ANOVA demonstrated significant differences

between white matter tracts for histological AxD ($F = 114.00$, $p < 0.001$), while the intra-axonal volume fraction shows no significant difference between different white matter tracts ($F = 0.79$, $p = 0.57$). The cross-animal variations are consistent with previous studies that used the same histological protocol (Harkins et al., 2012). Note that both biological variability and the sampling differences contributed to these variations. Histological images of six different white matter tracts of a representative rat spinal cord are shown in Figure 1, in which the corresponding segmented images are also provided (the second row). The white regions represent axons, black represents myelin and gray is extra-axonal space.

Histology-based computer simulations

The bottom row of Figure 1 shows the simulated apparent diffusion spectra arising from the intra- and extra-axonal spaces, respectively. Despite the large variations of axon shapes and sizes in each white matter tract, the simulated intra-axonal apparent diffusion spectra (red circles) can be fit well using Eq.(2) (red lines), which means the simplification of using cylinders with a unique mean AxD is plausible for interpreting OGSE measurements. The overall intra-axonal ADC values decrease from VST to dCST, consistent with the trend of mean axon diameter variations across these white matter tracts. The extra-axonal ADCs (blue diamonds) of six white matter tracts all clearly show a linear dependence on the gradient frequency (all $R^2 > 0.94$), which can be fit well with Eq.(3). Interestingly, the intra-axonal ADC is significantly larger than the extra-axonal ADC in VST, but decreases rapidly and eventually is smaller than extra-axonal ADC in dCST, while the extra-axonal ADC decreases slightly from VST to dCST. This suggests that even with the same MR parameters, e.g. gradient frequency (diffusion time), the relative contributions of intra- and extra-axonal spaces are heavily dependent on the axon dimensions. It has been suggested that water molecules may be more restricted in the extracellular space than in the intracellular space (Shemesh et al., 2011). Our simulations clearly show that the extra-axonal diffusion spectra may be higher or lower than those of intra-axonal space, suggesting that the extra-axonal diffusion may be more or less restricted than the intra-axonal diffusion, depending on the specific compartment dimensions.

Figure 2 compares AxD values derived from histology with those from the fits to the simulated OGSE data, and their corresponding Bland-Altman plot. There is an obvious underestimation when the histology AxD values are larger than ~6 μm or smaller than 1 μm, suggesting that the OGSE measurements under current experimental conditions can provide reliable fittings of AxD only in the range of 1 – 6 μm. Previous studies have shown a lower limit ~2.5 μm using the ActiveAx model (Dyrby et al., 2013), which means it is incapable of differentiating axons smaller than 2.5 μm but can only identify them as small. However, note that the maximum gradient strengths used in these two studies are different. It would be more relevant to compare the ability of fitting AxD using the current OGSE method with that of the ActiveAx model under the same experimental conditions. Nevertheless, the OGSE method used in the current study significantly pushed the detection limit down to 1 μm, which is slightly lower than the smallest mean AxD of all white matter tracts, i.e. 1.27 μm in dCST tract (see Table 1).

MRI and data fitting

Figure 3 shows diffusion-weighted signal attenuations (markers) of six different white matter tracts from a representative spinal cord. All signal attenuations were well fit using Eq.(1) (solid lines). For each white matter tract, higher gradient frequencies resulted in larger signal attenuations, while for each single frequency, diffusion signals were less attenuated in white matter tracts with smaller mean AxD. These results are expected because water molecules encounter less restricting boundaries at higher frequencies (shorter diffusion times) and/or in larger axons.

Figure 4 shows fitted parametric maps of the white matter of a representative spinal cord. The parametric maps of all other spinal cords were similar. Note that different regions of white matter tracts can be easily identified on the fitted mean AxD map, which is consistent with previous results of mouse spinal cords that employed gradient strength up to 4800 G/cm (Ong et al., 2008). However, previously reported displacement maps of fixed rat spinal cords obtained using conventional **q**-space imaging did not show such a clear contrast within white matter regions (Anaby et al., 2013; Assaf et al., 2000). This is presumably because the long diffusion times used in those studies (> 22ms and $\geqslant$ 30ms respectively) decreased the sensitivity for distinguishing small mean axon size differences among different white matter tracts. Note that these two studies used maximum gradient strengths of 117.5 G/cm and 150 G/cm, respectively, which were similar to the maximum gradient strength 133 G/cm used in the current study.

By contrast, the fitted f_{in} is more homogeneous across the whole white matter region. This is consistent with our histological findings that different white matter tracts have different mean AxD but similar f_{in} (see Table 1). The other parametric maps do not show clear contrasts for differentiating white matter tracts. Note that the estimated values of D_{in} in the dCST tract are markedly higher than those of other regions (see Figure 4 and Table 2). This is because the AxD in dCST is very small. Under such circumstances, the sensitivity to D_{in} is lower and may result in biased values, as experimentally confirmed in previous microcapillary studies (Li et al., 2014). The β_{ex} map is relatively homogeneous but shows a pattern that is inconsistent with the map of AxD. Although β_{ex} may not be simply related to any specific physical structure in the tissues, in general the slope of the ADC with frequency is itself an indicator of compartment size, and extra-axonal spaces may in general be larger when the axons are larger. The fitted D_{in}, D_{ex0} and β_{ex} values of all white matter tracts are tabulated in Table 2.

Figure 5 shows the Bland-Altman plots of the differences between the mean AxD (Figure 5.A) and f_{in} (Figure 5.B) fitted from OGSE measurements vs. those obtained from histology. All differences between the fitted mean AxD and f_{in} and those from histology are in very good agreement (within the range of ± 1.96 SD) except for one or two outliers. This indicates that both mean AxD and f_{in} have been fit accurately from the OGSE measurements non-invasively, consistent with histology.

Figure 6 shows the correlations of five fitted parameters, i.e. AxD, f_{in}, D_{in}, D_{ex0}, and β_{ex}, from all 36 ROI's with the corresponding mean AxD obtained from histology. The correlation coefficient r and p values obtained using the linear mixed-effects models are

provided for each correlation pair. The fitted and histological AxD's are in good correlation, r = 0.916 and p < 0.001. The identity line (perfect matching) deviates from the data when AxD > ~ 5 μm, suggesting the OGSE method underestimates the larger axons. The fitted f_{in} and D_{ex0} show no correlations with histology AxD with p = 0.687, and 0.184, respectively, By contrast, the fitted D_{in} and β_{ex} show a correlation with histology AxD with r = −0.343, p = 0.018 and r = 0.478, p < 0.001. We analyzed the intra-animal errors of AxD in two ways: the standard deviations of fitted AxD across each ROI and the propagation error based on the numerically estimated model Jacobians and residuals from the non-linear regressions. Both methods showed standard errors per pixel were in the range of 0.1–1μm across different white matter tracts and animals. Considering the number of pixels in each ROI is ~100, the standard errors per ROI are in the range of 0.01–0.1μm, which are much smaller than the inter-animal variations. Note that when axon size is small, the estimated D_{in} using OGSE methods could be significantly biased (Li et al., 2014). The correlation between β_{ex} and AxD could be explained by the increasing mean restricting distance in the extracellular space when mean axon size increase, even though β_{ex} as derived theoretically may not be clearly related to any physical structure in the tissues. In summary, these results suggest that f_{in} is an independent parameter from AxD, presumably because f_{in} is determined by axon counts and AxD together. Therefore, mapping both the mean AxD and f_{in} provides more comprehensive information about nervous tissue morphology.

DISCUSSION

Mapping mean AxD or AxD distributions has significant clinical and research potential to provide information about nerve microstructure. Previous diffusion MRI measurements of AxD used PGSE-based methods, such as those based on measuring displacement probability profiles from **q**-space imaging or the AxCaliber framework. These methods employ relatively long diffusion times, e.g. > 20 ms, and hence the corresponding root mean square displacement is larger than 8.9 μm if the diffusion coefficient is 2 μm^2/ms. Such a characteristic length is much larger than most axon diameters in the central nervous system, and therefore these PGSE-based methods have low sensitivity to distinguish small axons. To enhance the sensitivity to small axons, very high *q* values must be used which requires strong gradient strengths that may not be feasible *in vivo* (Ong and Wehrli, 2010; Ong et al., 2008). Another approach, the double-pulsed field gradient (d-PFG), was reported to probe AxD (Komlosh et al., 2013; Weber et al., 2009) with relatively weak gradients (Morozov et al., 2013), but it has also been shown that this d-PFG method is actually equivalent to the conventional PGSE method for zero mixing time and low diffusion weighting (Jespersen, 2012). The current study investigates a different approach, the OGSE method, to measure the mean AxD non-invasively. Instead of using high *q* values, much shorter diffusion times were achieved by tuning gradient frequencies. For example, the highest frequency (250 Hz) used in the current study corresponds to an effective diffusion time of 1 ms and root mean square displacement of 1.9 μm, which is comparable to small axon diameters. Therefore, the sensitivity to small axons is significantly enhanced in the OGSE measurements. In addition to an early feasibility study via computer simulations (Xu et al., 2009b), some attempts using OGSE-like sequences have been made to map mean axon size directly (Siow et al., 2013) and indirectly (apparent compartment size) (Shemesh et al., 2013), but neither of

these studies provided information on intra-axonal volume fraction. To the best of our knowledge, this is the first comprehensive OGSE study describing the measurement of both mean axon diameter and intra-axonal volume fraction with histological validation. In addition, this is also the first OGSE study that implements frequency-dependent models for extra-axonal diffusion in the quantitative fitting of axon diameter.

Water exchange

The water exchange between intra- and extra-axonal spaces was assumed negligible in the current study. The signal arising from myelin was assumed to be negligible due to low T_2 and relatively long echo times used in the OGSE measurements. These assumptions have been used in previous diffusion studies in fitting AxD, and reasonable results were obtained (Alexander et al., 2010; Assaf et al., 2008; Barazany et al., 2009; Ong and Wehrli, 2010). Moreover, the OGSE measurements probe much shorter diffusion times, and hence the effect of water exchange on OGSE diffusion measurements should be even less pronounced. However, the precise influence of water exchange on MR measurements remains controversial. Previous multiple-exponential T_2 measurements (Dula et al., 2010; Harkins et al., 2012) and OGSE numerical simulations (Xu et al., 2011a) suggest that the water exchange between myelin and intra-/extra-axonal spaces cannot strictly be ignored. By contrast, other studies have reported that intra-axonal water lifetimes are orders of magnitude higher than the diffusion times employed in the present study, suggesting the influence of water exchange on OGSE measurements is minor (Nilsson et al., 2013a; Sønderby et al., 2013). Nevertheless, it is plausible to consider the possibility of water exchange effects when implementing future OGSE measurements, especially when some morphologic variations may change water exchange rate. If necessary, modified Karger models can be used to account for the water exchange between different compartments (e.g. Kärger et al., 1988).

Co-registration of MR and histology images

In the current study, both the ROI's of all white matter tracts on the diffusion MR images and the corresponding regions of those white matter tracts on the histological images were chosen manually. Although this approach has also been used in previous diffusion studies in spinal cord *ex vivo* (Assaf et al., 2008; Chin et al., 2004; Ong and Wehrli, 2010; Ong et al., 2008; Schwartz et al., 2005b), it prevents a pixel-based comparison between the MR images and corresponding histology across an entire tissue sample, and hence the inter-sample variations can be enlarged due to sampling errors. For example, the comparison of results may be influenced by the specific choices of regions decided by the operator. Golabchi et al. proposed an approach that can perform a pixel-based comparison across the whole fixed spinal cord, at a cost of a relatively low spatial resolution of the histology images (0.53 μm in that study vs 0.075 μm in the current work) and hence the estimation of small axons (especially those in dCST) may be significantly biased. Moreover, the histology sections may not be cut exactly perpendicular to the axis of spinal cord tracts, which in turn may also cause biased estimations. 3D OGSE measurements and histology analyses may overcome these effects, but an accurate and sophisticated imaging co-registration procedure covering in vivo applications should be used (Choe et al., 2011).

Resolution limit

The resolution limit is an important metric to evaluate the accuracy of diffusion measurements for fitting AxD (Nilsson et al., 2013b). Previous studies have shown that the ActiveAx model has a resolution lower limit of ~2.5 μm and an upper limit ~10 μm with maximum gradient strength < 30 G/cm. This suggests that any axons smaller than 2.5 μm cannot be distinguished. By contrast, the OGSE method used in the current study has resolution lower limit down to 1 μm, which in turn provides the ability to fit the mean AxD of all white matter tracts reliably. However, we should recall that the maximum gradient strengths used in previous ActiveAx studies were much smaller than the current 133 G/cm. Hence, a direct comparison between ActiveAx and OGSE methods under the same experimental conditions would be of interest. Meanwhile, previous conventional **q**-space studies of rat spinal cords using similar maximum gradient strengths (Anaby et al., 2013; Assaf et al., 2000) did not provide clear contrast distinguishing white matter tracts as shown in the current study. This at least suggests that the OGSE method might be a preferred method compared with PGSE-based **q**-space imaging for detecting small axons. Note that, limited by the lowest frequency used, the upper limit for the OGSE method in the current study is ~ 5 μm, which is smaller than the upper limit (~10μm) of the ActiveAx model. This is because the diffusion time is not long enough to completely probe larger axons. Interestingly, a previous microcapillary phantom study suggested a cylinder size of 19 μm can be fit well using similar OGSE measurements (Li et al., 2014), while AxD > 5 μm were apparently underestimated with similar frequencies used in the current study. This is presumably because all cylinders in the phantom study had a unique diameter and signals arose from a single intra-cylinder compartment only. However, for the real biological tissues in the current study, the situation was more complicated. The axons were not perfect cylinders but had various shapes. The diameters of axons were not a unique size but a distribution of sizes. Moreover, the signals arose from two compartments, i.e. intra- and extra-axonal spaces. All of these complications challenged the fitting. Although the mean axon diameter 1–5 μm can be fit well, larger axons were underestimated. This suggests that other realistic features of biological tissues, e.g. axon shape, distribution of sizes, volume fraction, etc., should be considered to investigate the resolution limit of diffusion measurements in practice. It would be of interest to combine both OGSE and PGSE measurements in the future to provide more comprehensive microstructural information over a larger range of axon sizes. In addition, note that the resolution limit reported was slightly dependent on the maximum gradient strength (Dyrby et al., 2013), so it is worthwhile investigating in future studies how the resolution limit of the OGSE method may change with gradient strength, as well as other effects such as SNR and T_2.

Practical limitations

The effective diffusion time of OGSE measurements is $1/(4f)$, while the OGSE b value is proportional to G^2/f^2. Therefore, to achieve sufficient diffusion weighting (b values), strong gradient strengths are required to probe very short diffusion times (high frequencies). This is the main practical limitation on OGSE measurements for accurate quantification of very small axons in human *in vivo*. Recently, more advanced human gradient coils have been developed that are significantly stronger than normal gradients, such as the Connectome coil

with strength up to 300 mT/m for human heads (Setsompop et al., 2013) and local planar gradients with order-of-magnitude greater strength (1000 mT/m) for a limited field-of-view (~16 cm) (Aksel et al., 2007). These hardware improvements would significantly enhance the ability of the OGSE method for accurate quantification of small axons in human *in vivo*. Even with current normal gradient coils with relatively low gradient strength, e.g. < 60mT/m per channel, OGSE measurements of human brain have already shed light on the characterization of neural tissues at small scales (Baron and Beaulieu, 2014; Van et al., 2014).

Potential improvements

The framework proposed in the current work can be extended without much effort to include the distribution of AxD, as shown in the AxCaliber model. However, our simulations show that the accurate mapping of AxD distribution requires more b values and a broader range of frequencies compared with those used in the current work (data not shown), which in turn increases the total scanning time.

Only two diffusion compartments (intra- and extra-axonal diffusion) were considered in the current study which is appropriate for healthy spinal cord white matter tissues. However, it is also possible to include the isotropic diffusion from glial cells (Stanisz et al., 1997) and free diffusion, such as in CSF (Barazany et al., 2009) to better fit the diffusion data (Ferizi et al., 2013). Note that both intra- and extra-axonal diffusion are restricted so that their diffusion spectra are dependent on the gradient frequency. By contrast, the diffusion spectrum of the free water component is constant cross over all gradient frequencies. Therefore, it is expected that free water can be differentiated well from restricted diffusion components using OGSE measurements with multiple gradient frequencies. This alone could be significant for various applications *in vivo* (Pasternak et al., 2009).

The diffusion gradients were applied perpendicular to the main axes of the spinal cords in the current study. However, in the spinal cord there are some fiber populations that cross in the transverse plane, for which our model does not account. In addition, the undulation of white matter tracts can also bias the estimation of mean axon diameter (Nilsson et al., 2012). Implementing multiple-directional tensor imaging with the OGSE method will not only solve this problem but also make the measurements of mean axon diameter using OGSE methods feasible in neural tissue with white matter fibers in arbitrary directions, e.g. in brain.

The number of acquisitions averaged was chosen to be 80 in the current study in order to fulfill an overnight scan. Baron and Beaulieu (2014) reported that SNR of OGSE measurements in the human brain *in vivo* can reach ~ 50 with the number of acquisitions averaged = 6, and a 30-direction DTI measurement using the OGSE method can be completed within 10 min, which is clinically feasible. Therefore, one next step is to investigate the requirement of SNR for accurate fitting using the framework proposed in the current work. Here, we used 21 data points (in addition to the b=0 image, there were five frequencies and four non-zero b values) in each fitting to obtain mean AxD and f_{in}. A possible direction is to evaluate whether the number of diffusion-weighted signals required to estimate the mean axon diameter can be reduced (Alexander, 2008). The minimal number

of b values and number of acquisitions averaged needed for adequate fitting accuracy and precision need to be established and optimized (Li et al., 2010).

CONCLUSIONS

The oscillating gradient spin echo (OGSE) method with the ability to probe short diffusion length scales was implemented to map mean axon diameters and intra-axonal space volume fractions of rat spinal white matter tracts. Appropriate models to describe intra- and extra-axonal diffusion were proposed and validated using histological-image-based computer simulations. These models were then implemented to successfully fit mean axon diameter and intra-axonal space volume fractions. Despite some underestimation of the diameters of large axons (e.g. > 5 μm), the overall fitted values were in good agreement with histology, including those small axons with diameters in the range from 1 to 2.5 μm. This work establishes a framework for quantitatively characterizing white matter morphology using the OGSE method with high sensitivity to small axons.

ACKNOWLEDGEMENTS

This study was supported by NIH K25CA168936, R01CA109106, R01CA173593, R01EB001744 and P50CA128323. The authors thank Dr. William M. Valentine for providing the light microscopy. Tissue preparation for histology was performed in part through the use of the VUMC Cell Imaging Shared Resource.

REFERENCES

Aggarwal M, Jones MV, Calabresi PA, Mori S, Zhang J. Probing mouse brain microstructure using oscillating gradient diffusion MRI. Magn Reson Med. 2012; 67:98–109. [PubMed: 21590726]

Aksel B, Marinelli L, Collick BD, Von Morze C, Bottomley PA, Hardy CJ. Local planar gradients with order-of-magnitude strength and speed advantage. Magn Reson Med. 2007; 58:134–143. [PubMed: 17659620]

Alexander DC. A general framework for experiment design in diffusion MRI and its application in measuring direct tissue-microstructure features. Magn Reson Med. 2008; 60:439–448. [PubMed: 18666109]

Alexander DC, Hubbard PL, Hall MG, Moore Ea, Ptito M, Parker GJM, Dyrby TB. Orientationally invariant indices of axon diameter and density from diffusion MRI. Neuroimage. 2010; 52:1374–1389. [PubMed: 20580932]

Anaby D, Duncan ID, Smith CM, Cohen Y. q-Space diffusion MRI (QSI) of the disease progression in the spinal cords of the Long Evans shaker: diffusion time and apparent anisotropy. NMR Biomed. 2013; 26:1879–1886. [PubMed: 24123305]

Andrews TJ, Osborne MT, Does MD. Diffusion of myelin water. Magn Reson Med. 2006; 56:381–385. [PubMed: 16767712]

Assaf Y, Blumenfeld-Katzir T, Yovel Y, Basser PJ. AxCaliber: a method for measuring axon diameter distribution from diffusion MRI. Magn Reson Med. 2008; 59:1347–1354. [PubMed: 18506799]

Assaf Y, Cohen Y. Assignment of the water slow-diffusing component in the central nervous system using q-space diffusion MRS: implications for fiber tract imaging. Magn Reson Med. 2000; 43:191–199. [PubMed: 10680682]

Assaf Y, Freidlin RZ, Rohde GK, Basser PJ. New modeling and experimental framework to characterize hindered and restricted water diffusion in brain white matter. Magn Reson Med. 2004; 52:965–978. [PubMed: 15508168]

Assaf Y, Mayk A, Cohen Y. Displacement Imaging of Spinal Cord Using q-Space Diffusion Weighted MRI. Magn Reson Imaging. 2000; 44:713–722.

Barazany D, Basser PJ, Assaf Y. In vivo measurement of axon diameter distribution in the corpus callosum of rat brain. Brain. 2009; 132:1210–1220. [PubMed: 19403788]

Baron, Ca; Beaulieu, C. Oscillating Gradient Spin-Echo (OGSE) diffusion tensor imaging of the human brain. Magn Reson Med. 2014 (in press).

Brun A, Englund E. A white matter disorder in dementia of the Alzheimer type: a pathoanatomical study. Ann Neurol. 1986; 19:253–262. [PubMed: 3963770]

Callaghan P, Coy A, MacGowan D. Diffraction-like effects in NMR diffusion studies of fluids in porous solids. Nature. 1991; 351:467–469.

Chin C, Wehrli FW, Hwang SN, Takahashi M, Hackney DB. Biexponential Diffusion Attenuation in the Rat Spinal Cord□: Computer Simulations Based on Anatomic Images of Axonal Architecture. Magn Reson Med. 2002; 47:455–460. [PubMed: 11870831]

Chin CL, Wehrli FW, Fan Y, Hwang SN, Schwartz ED, Nissanov J, Hackney DB. Assessment of axonal fiber tract architecture in excised rat spinal cord by localized NMR q-space imaging: simulations and experimental studies. Magn Reson Med. 2004; 52:733–740. [PubMed: 15389948]

Choe AS, Gao Y, Li X, Compton KB, Stepniewska I, Anderson AW. Accuracy of image registration between MRI and light microscopy in the ex vivo brain. Magn Reson Imaging. 2011; 29:683–692. [PubMed: 21546191]

Colvin DC, Jourquin J, Xu J, Does MD, Estrada L, Gore JC. Effects of intracellular organelles on the apparent diffusion coefficient of water molecules in cultured human embryonic kidney cells. Magn Reson Med. 2011a; 65:796–801. [PubMed: 21337411]

Colvin DC, Loveless ME, Does MD, Yue Z, Yankeelov TE, Gore JC. Earlier detection of tumor treatment response using magnetic resonance diffusion imaging with oscillating gradients. Magn Reson Imaging. 2011b; 29:315–323. [PubMed: 21190804]

Cory DG, Garroway AN. Measurement of translational displacement probabilities by NMR: an indicator of compartmentation. Magn Reson Med. 1990; 14:435–444. [PubMed: 2355827]

Denef JF, Cordier AC, Mesquita M, Haumont S. The Influence of Fixation Procedure, Embedding Medium and Section Thickness on Morphometric Data in Thyroid Gland. Histochemistry. 1979; 63:163–171. [PubMed: 115814]

Does MD, Parsons EC, Gore JC. Oscillating gradient measurements of water diffusion in normal and globally ischemic rat brain. Magn Reson Med. 2003; 49:206–215. [PubMed: 12541239]

Dula AN, Gochberg DF, Valentine HL, Valentine WM, Does MD. Multiexponential T2, magnetization transfer, and quantitative histology in white matter tracts of rat spinal cord. Magn Reson Med. 2010; 63:902–909. [PubMed: 20373391]

Dyrby TB, Søgaard LV, Hall MG, Ptito M, Alexander DC. Contrast and stability of the axon diameter index from microstructure imaging with diffusion MRI. Magn Reson Med. 2013; 70:711–721.

Ferizi U, Schneider T, Panagiotaki E, Nedjati-Gilani G, Zhang H, Wheeler-Kingshott Ca M, Alexander DC. A ranking of diffusion MRI compartment models with in vivo human brain data. Magn Reson Med. 2013

Ford JC, Hackney DB. Numerical model for calculation of apparent diffusion coefficients (ADC) in permeable cylinders--comparison with measured ADC in spinal cord white matter. Magn Reson Med. 1997; 37:387–394. [PubMed: 9055229]

Glovinsky Y, Quigley Ha, Dunkelberger GR. Retinal ganglion cell loss is size dependent in experimental glaucoma. Invest Ophthalmol Vis Sci. 1991; 32:484–491. [PubMed: 2001923]

Gore JC, Xu J, Colvin DC, Yankeelov TE, Parsons EC, Does MD. Characterization of tissue structure at varying length scales using temporal diffusion spectroscopy. NMR Biomed. 2010; 23:745–756. [PubMed: 20677208]

Gross B, Kosfeld R. Anwendung der spin-echo-methode der messung der selbstdiffusion. Messtechnik. 1969; 77:171–177.

Gullapalli J, Krejza J, Schwartz ED. In vivo DTI evaluation of white matter tracts in rat spinal cord. J Magn Reson imaging. 2006; 24:231–234. [PubMed: 16767707]

Harkins KD, Dula AN, Does MD. Effect of intercompartmental water exchange on the apparent myelin water fraction in multiexponential T2 measurements of rat spinal cord. Magn Reson Med. 2012; 67:793–800. [PubMed: 21713984]

Jespersen SN. Equivalence of double and single wave vector diffusion contrast at low diffusion weighting. NMR Biomed. 2012; 25:813–818. [PubMed: 22134913]

Kärger, J.; Pfeifer, H.; Heink, W. Principles and applications of self-diffusion measurements by nuclear magnetic resonance. In: Waugh, JS., editor. Advances in Magnetic Resonance. Academic Press, Inc., 1250 Sixth Avenue San Diego, California 92101; 1988. p. 1-89.

Kershaw J, Leuze C, Aoki I, Obata T, Kanno I, Ito H, Yamaguchi Y, Handa H. Systematic changes to the apparent diffusion tensor of in vivo rat brain measured with an oscillating-gradient spin-echo sequence. Neuroimage. 2013; 70:10–20. [PubMed: 23274188]

Komlosh ME, Özarslan E, Lizak MJ, Horkayne-Szakaly I, Freidlin RZ, Horkay F, Basser PJ. Mapping average axon diameters in porcine spinal cord white matter and rat corpus callosum using d-PFG MRI. Neuroimage. 2013; 78:210–216. [PubMed: 23583426]

Lam, WW.; Jbabdi, S.; Miller, KL. A model for extra-axonal diffusion spectra; Proceedings 22nd Scientific Meeting, International Society for Magnetic Resonance in Medicine; 2014. p. 395

Lätt J, Nilsson M, Malmborg C, Rosquist H, Wirestam R, Ståhlberg F, Topgaard D, Brockstedt S. Accuracy of q-space related parameters in MRI: simulations and phantom measurements. IEEE Trans Med Imaging. 2007; 26:1437–1447. [PubMed: 18041259]

Li H, Gore JC, Xu J. Fast and robust measurement of microstructural dimensions using temporal diffusion spectroscopy. J Magn Reson. 2014; 242:4–9. [PubMed: 24583517]

Li K, Zu Z, Xu J, Janve VA, Gore JC, Does MD, Gochberg DF. Optimized inversion recovery sequences for quantitative T1 and magnetization transfer imaging. Magn Reson Med. 2010; 64:491–500. [PubMed: 20665793]

Lovas G, Szilágyi N, Majtényi K, Palkovits M, Komoly S. Axonal changes in chronic demyelinated cervical spinal cord plaques. Brain. 2000; 123(Pt 2):308–317. [PubMed: 10648438]

Morozov D, Bar L, Sochen N, Cohen Y. Measuring small compartments with relatively weak gradients by angular double-pulsed-field-gradient NMR. Magn Reson Imaging. 2013; 31:401–407. [PubMed: 23102951]

Nilsson M, Lätt J, Ståhlberg F, van Westen D, Hagslätt H. The importance of axonal undulation in diffusion MR measurements: a Monte Carlo simulation study. NMR Biomed. 2012; 25:795–805. [PubMed: 22020832]

Nilsson M, Lätt J, van Westen D, Brockstedt S, Lasič S, Ståhlberg F, Topgaard D. Noninvasive mapping of water diffusional exchange in the human brain using filter-exchange imaging. Magn Reson Med. 2013a; 69:1573–1581. [PubMed: 22837019]

Nilsson M, van Westen D, Ståhlberg F, Sundgren PC, Lätt J. The role of tissue microstructure and water exchange in biophysical modelling of diffusion in white matter. MAGMA. 2013b; 26:345–370. [PubMed: 23443883]

Novikov DS, Fieremans E, Jensen JH, Helpern JA. Random walk with barriers. Nat Phys. 2011; 7:508–514. [PubMed: 21686083]

Novikov DS, Fieremans E, Jensen JH, Helpern JA. Characterizing microstructure of living tissues with time-dependent diffusion. arXiv:1210.3014v1. 2012

Novikov DS, Jensen JH, Helpern JA, Fieremans E. Revealing mesoscopic structural universality with diffusion. Proc Natl Acad Sci U S A. 2014

Ong HH, Wehrli FW. Quantifying axon diameter and intra-cellular volume fraction in excised mouse spinal cord with q-space imaging. Neuroimage. 2010; 51:1360–1366. [PubMed: 20350604]

Ong HH, Wright AC, Wehrli SL, Souza A, Schwartz ED, Hwang SN, Wehrli FW. Indirect measurement of regional axon diameter in excised mouse spinal cord with q-space imaging: simulation and experimental studies. Neuroimage. 2008; 40:1619–1632. [PubMed: 18342541]

Parsons EC Jr. Does MD, Gore JC. Temporal diffusion spectroscopy: theory and implementation in restricted systems using oscillating gradients. Magn Reson Med. 2006; 55:75–84. [PubMed: 16342147]

Pasternak O, Sochen N, Gur Y, Intrator N, Assaf Y. Free water elimination and mapping from diffusion MRI. Magn Reson Med. 2009; 62:717–730. [PubMed: 19623619]

Payne SC, Bartlett Ca, Harvey AR, Dunlop Sa, Fitzgerald M. Myelin sheath decompaction, axon swelling, and functional loss during chronic secondary degeneration in rat optic nerve. Invest Ophthalmol Vis Sci. 2012; 53:6093–6101. [PubMed: 22879411]

Portnoy S, Flint JJ, Blackband SJ, Stanisz GJ. Oscillating and pulsed gradient diffusion magnetic resonance microscopy over an extended b-value range: Implications for the characterization of tissue microstructure. Magn Reson Med. 2012; 69:1131–1145. [PubMed: 22576352]

Ritchie JM. On the relation between fibre diameter and conduction velocity in myelinated nerve fibres. Proc R Soc Lond B Biol Sci. 1982; 217:29–35. [PubMed: 6131421]

Schwartz ED, Cooper E, Fan Y, Jawad A. MRI diffusion coefficients in spinal cord correlate with axon morphometry. Neuroreport. 2005a; 16:73–76. [PubMed: 15618894]

Schwartz ED, Cooper ET, Chin C-L, Wehrli S, Tessler A, Hackney DB. Ex vivo evaluation of ADC values within spinal cord white matter tracts. AJNR Am J Neuroradiol. 2005b; 26:390–397. [PubMed: 15709142]

Setsompop K, Kimmlingen R, Eberlein E, Witzel T, Cohen-Adad J, McNab JA, Keil B, Tisdall MD, Hoecht P, Dietz P, Cauley SF, Tountcheva V, Matschl V, Lenz VH, Heberlein K, Potthast A, Thein H, Van Horn J, Toga A, Schmitt F, Lehne D, Rosen BR, Wedeen V, Wald LL. Pushing the limits of in vivo diffusion MRI for the Human Connectome Project. Neuroimage. 2013; 80:220–233. [PubMed: 23707579]

Shemesh N, Adiri T, Cohen Y. Probing microscopic architecture of opaque heterogeneous systems using double-pulsed-field-gradient NMR. J Am Chem Soc. 2011; 133:6028–6035. [PubMed: 21446740]

Shemesh N, Alvarez Ga, Frydman L. Measuring small compartment dimensions by probing diffusion dynamics via Non-uniform Oscillating-Gradient Spin-Echo (NOGSE) NMR. J Magn Reson. 2013; 237:49–62. [PubMed: 24140623]

Shepherd TM, Thelwall PE, Stanisz GJ, Blackband SJ. Aldehyde fixative solutions alter the water relaxation and diffusion properties of nervous tissue. Magn Reson Med. 2009; 62:26–34. [PubMed: 19353660]

Siow B, Drobnjak I, Ianus A, Christie IN, Lythgoe MF, Alexander DC. Axon radius estimation with Oscillating Gradient Spin Echo (OGSE) Diffusion MRI. Diffus Fundam. 2013; 18:1–6.

Sønderby CK, Lundell HM, Søgaard LV, Dyrby TB. Apparent exchange rate imaging in anisotropic systems. Magn Reson Med. 2013 00.

Stanisz GJ, Szafer A, Wright GA, Henkelman RM. An analytical model of restricted diffusion in bovine optic nerve. Magn Reson Med. 1997; 37:103–111. [PubMed: 8978638]

Stepisnik J, Lasic S, Mohoric A, Sersa I, Sepe A. Spectral characterization of diffusion in porous media by the modulated gradient spin echo with CPMG sequence. J Magn Reson. 2006; 182:195–199. [PubMed: 16844392]

Szafer A, Zhong J, Gore JC. Theoretical model for water diffusion in tissues. Magn Reson Med. 1995; 33:697–712. [PubMed: 7596275]

Tang Y, Nyengaard JR. A stereological method for estimating the total length and size of myelin fibers in human brain white matter. J Neurosci Methods. 1997; 73:193–200. [PubMed: 9196291]

Van AT, Holdsworth SJ, Bammer R. In vivo investigation of restricted diffusion in the human brain with optimized oscillating diffusion gradient encoding. Magn Reson Med. 2014; 71:83–94. [PubMed: 23447055]

Van Putten EG, Akbulut D, Bertolotti J, Vos WL, Lagendijk a, Mosk a. P. Scattering Lens Resolves Sub-100 nm Structures with Visible Light. Phys Rev Lett. 2011; 106:193905. [PubMed: 21668161]

Weber T, Ziener CH, Kampf T, Herold V, Bauer WR, Jakob PM. Measurement of apparent cell radii using a multiple wave vector diffusion experiment. Magn Reson Med. 2009; 61:1001–1006. [PubMed: 19205023]

Wilkinson, a E.; Bridges, LR.; Sivaloganathan, S. Correlation of survival time with size of axonal swellings in diffuse axonal injury. Acta Neuropathol. 1999; 98:197–202. [PubMed: 10442560]

Xu J, Does MD, Gore JC. Numerical study of water diffusion in biological tissues using an improved finite difference method. Phys Med Biol. 2007; 52:N111–N126. [PubMed: 17374905]

Xu J, Does MD, Gore JC. Sensitivity of MR diffusion measurements to variations in intracellular structure: Effects of nuclear size. Magn Reson Med. 2009a; 61:828–833. [PubMed: 19205020]

Xu J, Does MD, Gore JC. Quantitative characterization of tissue microstructure with temporal diffusion spectroscopy. J Magn Reson. 2009b; 200:189–197. [PubMed: 19616979]

Xu J, Does MD, Gore JC. Dependence of temporal diffusion spectra on microstructural properties of biological tissues. Magn Reson Imaging. 2011a; 29:380–390. [PubMed: 21129880]

Xu, J.; Harkins, KD.; Horch, RA.; Does, MD.; Gore, JC. Dependence of Temporal Diffusion Spectroscopy on Axon Size in White Matter Tracts of Rat Spinal Cord; Melbourn, Australia. Proceedings of the 20th Annual Meeting of ISMRM; 2012a. p. 351

Xu, J.; Jeong, H-K.; Does, MD.; Anderson, AW.; Chen, L-M.; Gore, JC. Dependence of fractional anisotropy on diffusion time: a frequency-domain analysis using temporal diffusion spectroscopy; Stockholm, Sweden. Proceedings of the 18th Annual Meeting of ISMRM; 2010. p. 4038

Xu J, Li K, Smith RA, Waterton JC, Zhao P, Chen H, Does MD, Manning HC, Gore JC. Characterizing tumor response to chemotherapy at various length scales using temporal diffusion spectroscopy. PLoS One. 2012b; 7:e41714. [PubMed: 22911846]

Xu J, Xie J, Jourquin J, Colvin DC, Does MD, Quaranta V, Gore JC. Influence of cell cycle phase on apparent diffusion coefficient in synchronized cells detected using temporal diffusion spectroscopy. Magn Reson Med. 2011b; 65:920–926. [PubMed: 21413058]

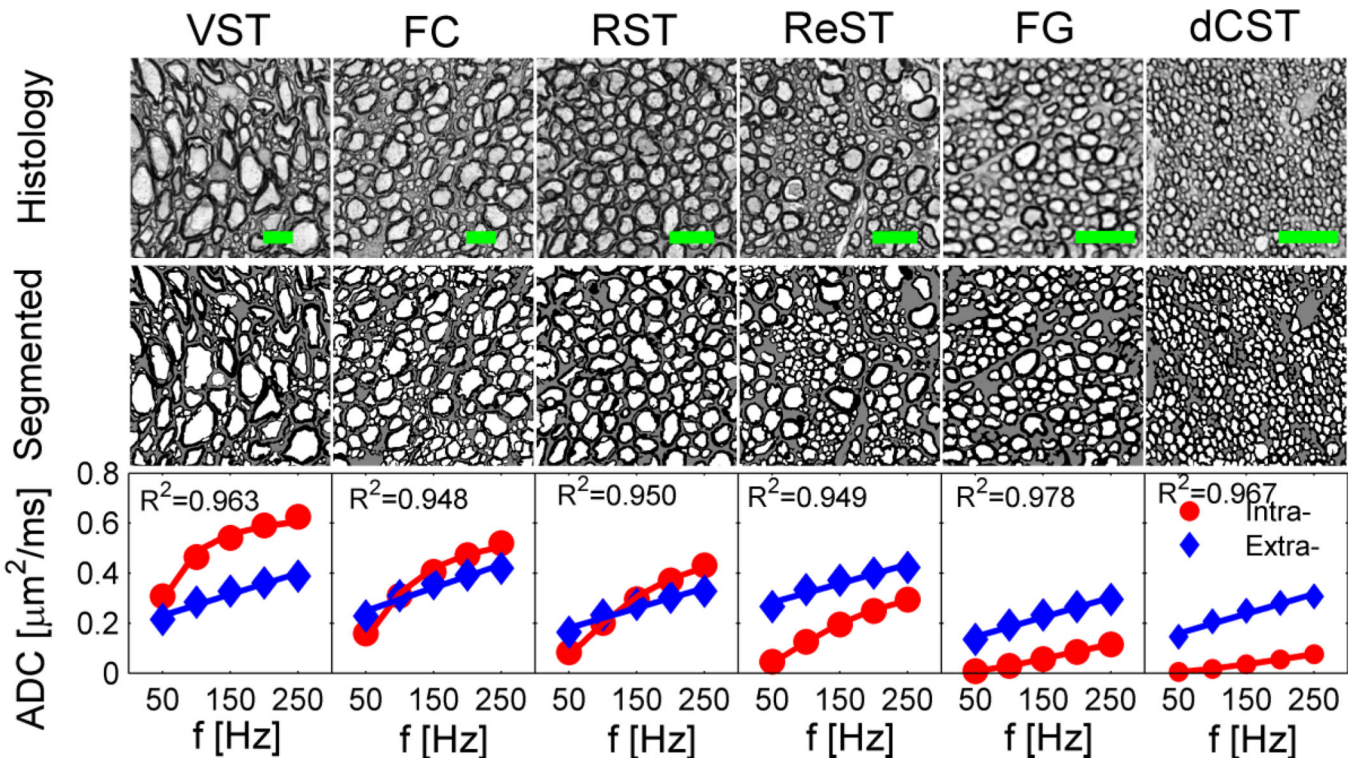

Figure 1.

Histological images (top row) and the corresponding segmented images (middle row) of six different white matter tracts of a representative rat spinal cord. The scale (green) bars represent 10 μm. The bottom row shows the corresponding simulated apparent diffusion spectra of the intra- (red circles) and extra-axonal (blue diamonds) spaces, respectively. The solid lines are fitted spectra using Eq.(2) and (3), respectively. R^2 values of the linear fitting to Eq.(3) are provided for each figure.

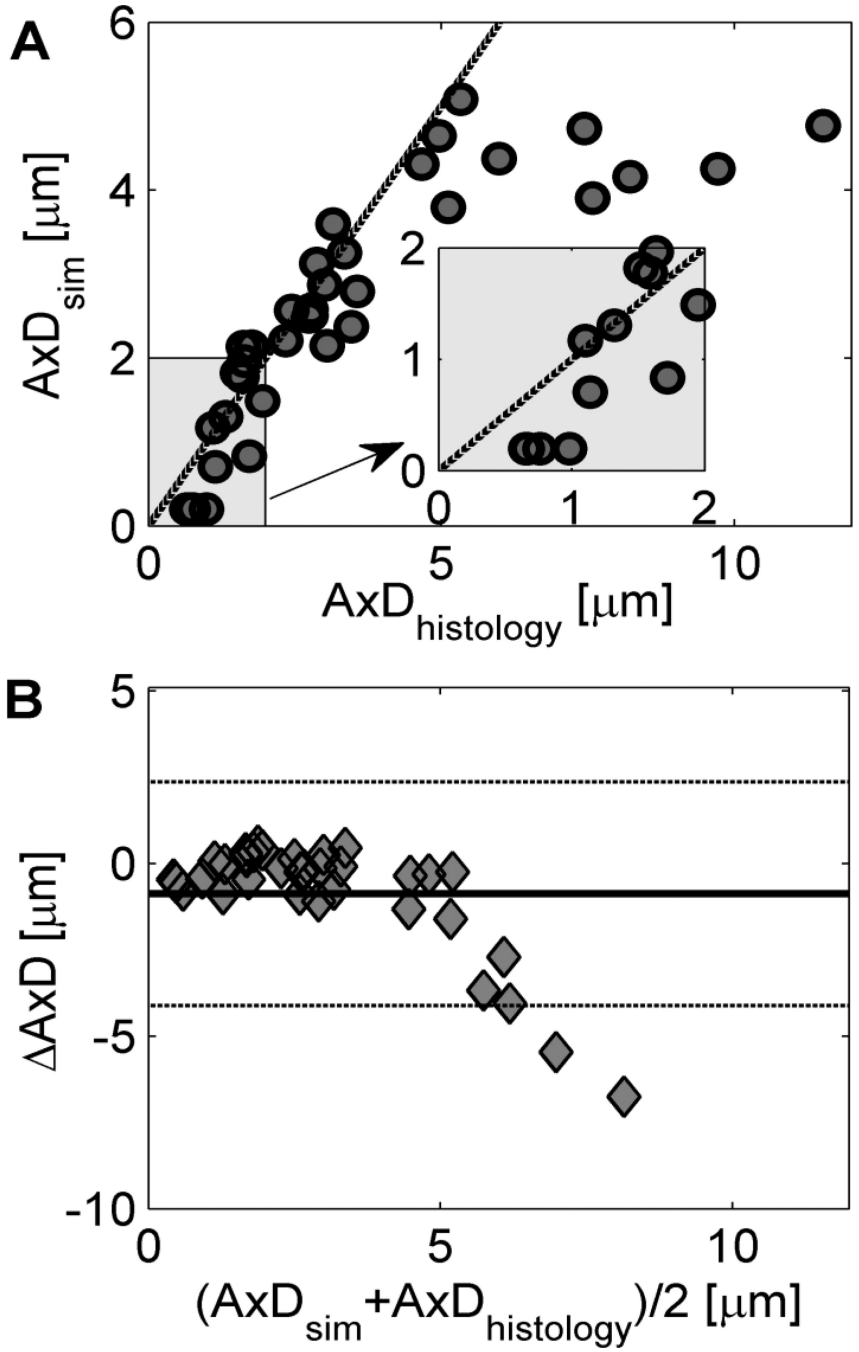

Figure 2.

(A) The scatter plot of histology AxD vs. fitted AxD from simulated OGSE signals. The dashed line represents the identity line. (B) The corresponding Bland-Altman plot of histology and fitted AxD. Note that the OGSE measurements provide reliable estimation of AxD in the range from ~1 μm to ~6 μm, while significantly underestimate axon size when AxD > 6 μm and cannot identify axons smaller than 1 μm.

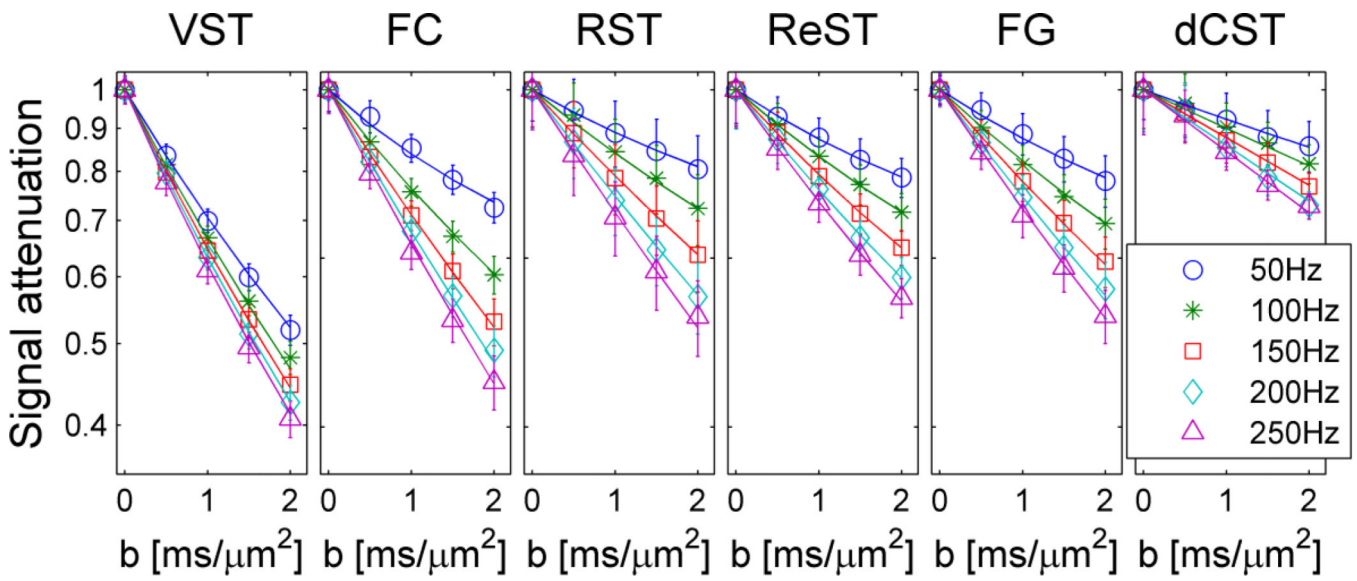

Figure 3.

The diffusion-weighted signal attenuations of six different white matter tracts from a representative rat spinal cord. Markers are mean signals and the error bars represent standard deviations of ROI signals. The solid lines are fitted results using Eq.(1).

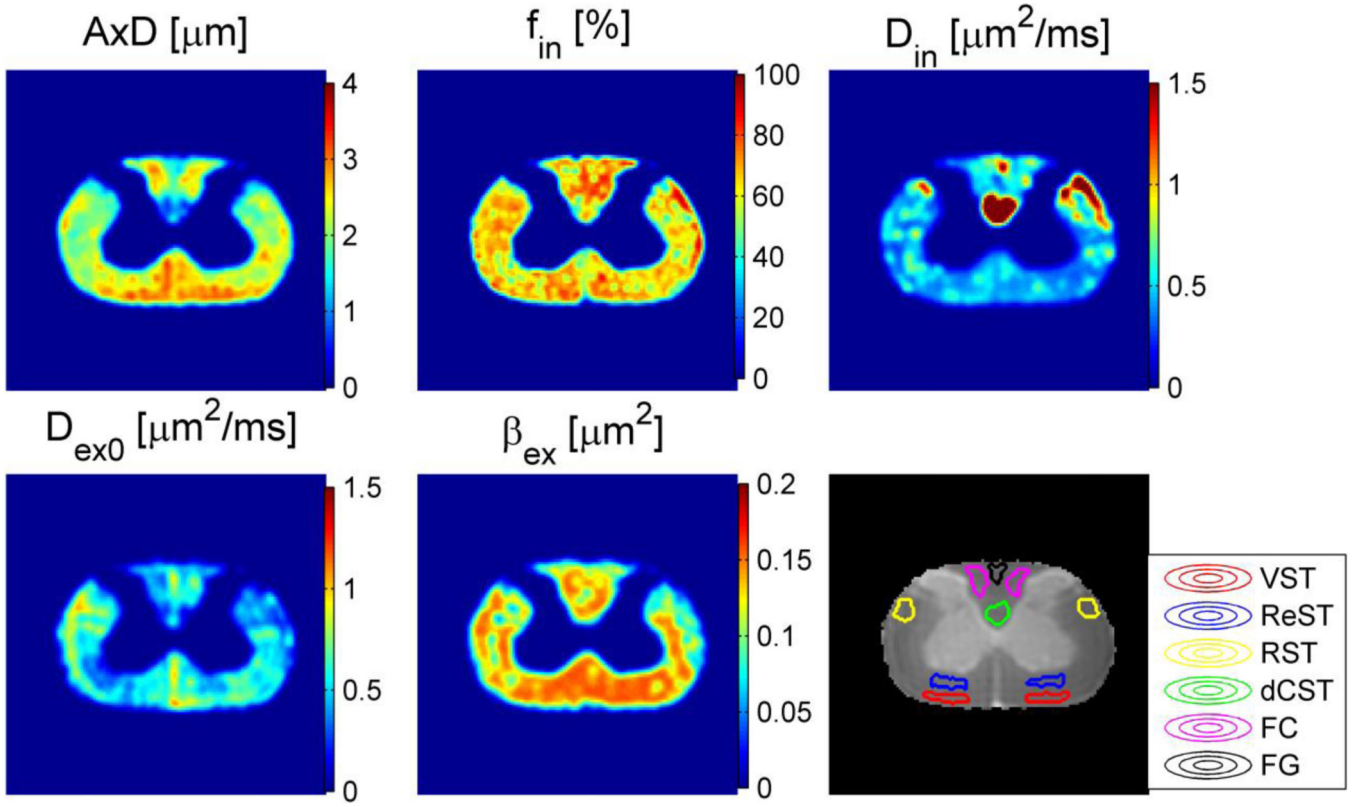

Figure 4.

Fitted five parametric maps of a representative rat spinal cord. The lower right figure is the T_2-weighted image overlaid with the ROI's of six different white matter tracts.

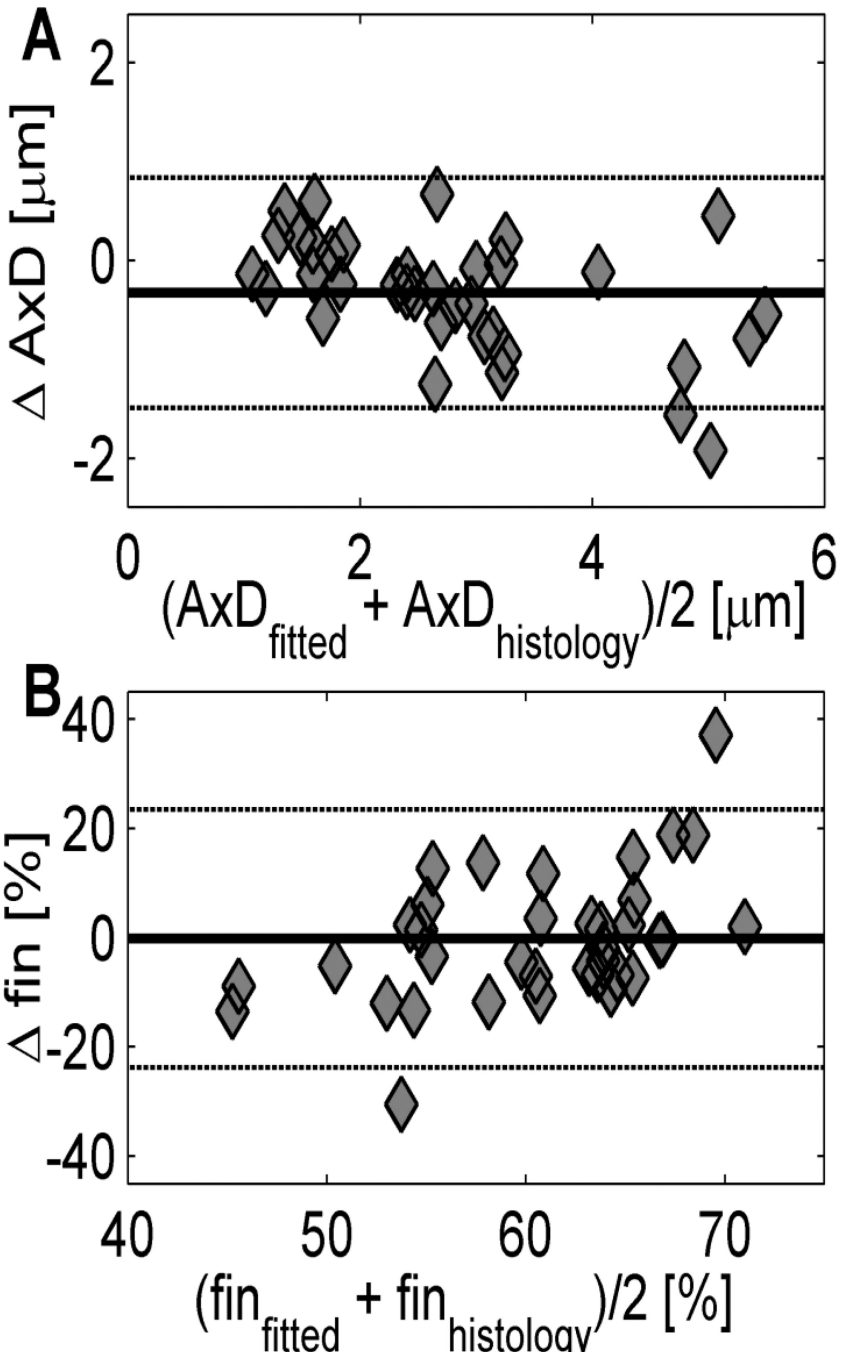

Figure 5.

The Bland-Altman plots of differences between the fitted and histology (A) AxD and (B) f_{in} from all 36 ROI's. The solid lines represent mean differences, and the dash lines represent mean differences ± 1.96 SD.

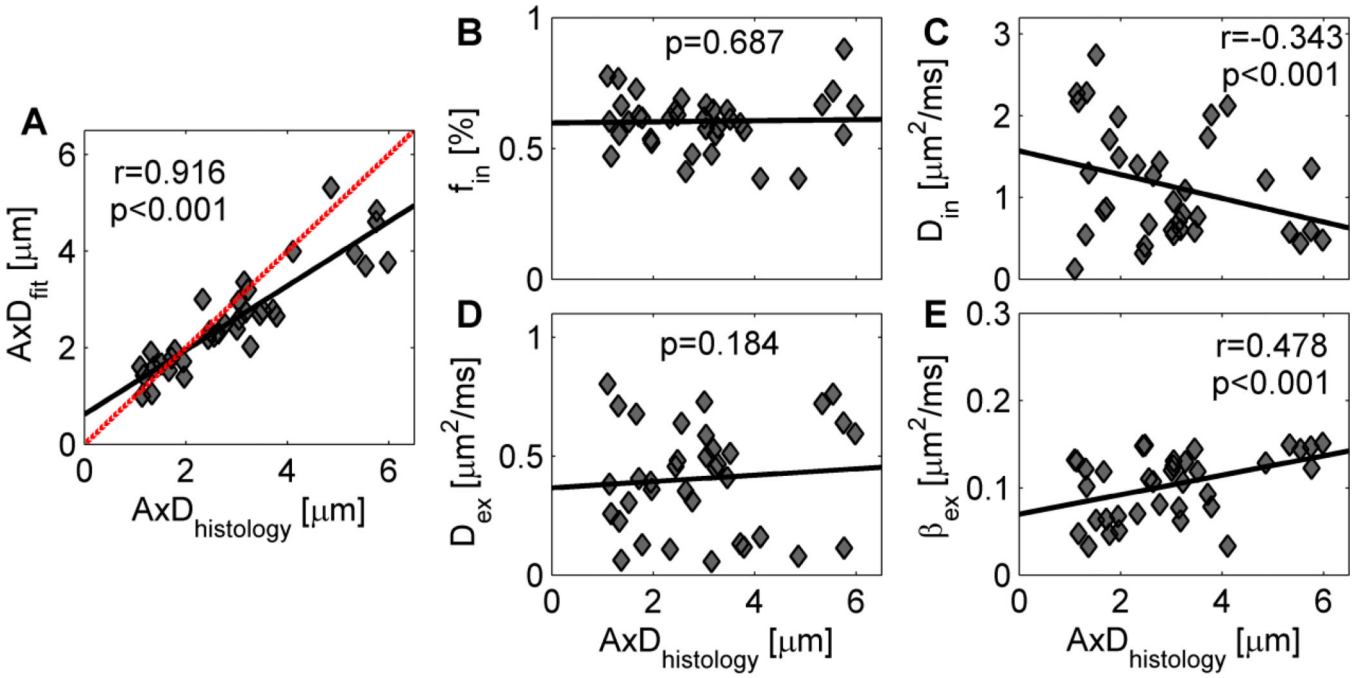

Figure 6.

The comparison of fitted five parameters, i.e. AxD, f_{in}, D_{in}, D_{ex0}, and β_{ex}, with the mean AxD obtained from histology. The black solid lines represent linear fitting, and the red dash line is the identity line, i.e. perfect matching. The correlation coefficient r and p values from linear mixed-effects models are provided for each correlation pair if $p < 0.05$.

Table 1

The area-weighted mean axon diameter (AxD)and effective intra-axonal water fraction (f_{in}) obtained from fittings and histology, and volume fractions for intra-/extra-axonal spaces and myelin and axon density of all six spinal cords obtained from histology. The values and errors represent the mean and standard deviations across all animals, respectively.

	Tracts	VST	FC	RST	ReST	FG	dCST
Fitted	*AxD* [μm]	4.63±0.55	2.91 ±0.49	2.67±0.33	2.53±0.48	1.71 ±0.20	1.39±0.27
	f_{in} [%]	64.51±15.15	58.80±9.60	58.47±6.39	56.01 ±8.61	63.28±9.05	61.22±9.48
Histology	*AxD* [μm]	5.54±0.36	3.52±0.36	3.06±0.37	2.72±0.36	1.73±0.22	1.27±0.15
	f_{in} [%]	59.67±7.32	63.50±6.08	57.33±10.84	55.00±8.85	60.33±3.40	62.00±4.97
	Intra-axonal fraction [%]	33.00±5.16	33.00±4.80	29.67±5.79	29.17±5.21	29.67±2.29	29.33±2.29
	Extra-axonal fraction [%]	22.33±3.64	18.83±3.58	21.83±5.84	23.67±4.68	19.17±2.67	18.33±3.20
	Myelin fraction [%]	44.50±1.98	48.17±5.05	48.50±3.15	47.17±2.19	50.83±4.06	52.17±2.79
	Axon density [10^5 mm^2]	0.65±0.16	0.93±0.23	1.00±0.32	1.33±0.24	1.89±0.49	3.44±0.41

Table 2

Summary of fitted D_{in}, D_{ex0} and β_{ex} values of all white matter tracts. The values and errors represent the mean and standard deviations across all animals, respectively.

Tracts	VST	FC	RST	ReST	FG	dCST
D_{in} [μm^2/ms]	0.78±0.36	1.11±0.68	1.03±0.41	0.86±0.41	1.24±0.52	1.82±0.87
D_{ex0} [μm^2/ms]	0.48±0.28	0.37±0.17	0.47±0.20	0.32±0.17	0.45±0.20	0.34±0.23
β_{ex} [μm^2]	0.14±0.01	0.09±0.04	0.11±0.02	0.11±0.03	0.08±0.03	0.08±0.04